EVALUATION OF REGIONAL OCEAN CIRCULATION MODELS FOR THE MEDITERRANEAN SEA AT THE STRAIT OF GIBRALTAR: VOLUME TRANSPORT AND THERMOHALINE PROPERTIES OF THE OUTFLOW

Javier Soto-Navarro[1], Samuel Somot[2], Florence Sevault[2], Jonathan Beuvier[2,3], Francisco Criado-Aldeanueva[1], Jesús García-Lafuente[1], Karine Béranger[4].

(1) Physical Oceanography Group of the University of Málaga (GOFIMA)

(2) Météo-France/CNRS, CNRM-GAME, 42 avenue Coriolis 31057 Toulouse, France.

(3) Mercator Océan

(4) UME, ENSTA-ParisTech

Abstract

A set of simulations from different configurations of the NEMOMED8, NEMOMED12 and NEMOMED36 ocean regional circulation models for the Mediterranean Sea has been studied in order to assess the accuracy of their representation of the exchange through the Strait of Gibraltar. The model volume transport and thermohaline properties of the Mediterranean outflow have been compared with observational data collected at Espartel sill, the westernmost sill of the strait, by a permanent station moored since October 2004 in the frame of the INGRES projects. Results show that, in terms of volume transport, NEMOMED8 simulations perform a better representation of the exchange, while NEMOMED12/36 underestimate both the mean inflow and outflow. The reason for this underestimation is a too low velocity of the flow, which could be consequence of an enhanced roughness effect due the flow-bathymetry interaction. An important improvement in the representation of the exchange seasonality is achieved by

the simulations including sea surface height variability of the Atlantic area of the domain. The results for the themohaline characteristics of the Mediterranean outflow are better for NEMOMED12 and NEMOMED36, as a consequence of their better representation of the local dynamical processes that leads to a more realistic composition of the Mediterranean waters comprising the flow.

1. Introduction

The characterization of the exchange through the Strait of Gibraltar is crucial to understand the functioning of the Mediterranean Sea due to its critical role in the closure of the water and heat budgets (Bethoux and Gentilli, 1999; Mariotti et al., 2002; Criado-Aldeanueva et al., 2012). The evaporation losses of the basin generate a water deficit that must be compensated by a net inflow of warm and fresher Atlantic waters, which are progressively transformed along the basin, becoming saltier and eventually sinking to intermediate and deep layers in convection processes triggered by winter cooling. Finally, the colder and saltier Mediterranean waters leave the basin through the strait. The close relationship between the circulation of the basin and the exchange through Gibraltar makes the modeling of the volume transport and the water mass properties of the exchanged flows a key factor in the development of regional circulation models for the Mediterranean Sea (Sannino et al., 2009).

The volume transport variability depends on the hydraulic characteristics of the strait, and can be described by two variables: the interface depth between the Mediterranean and Atlantic layers, h, and the flow velocity, u. In an ideal two-layer model of the strait, hydraulically controlled at Camarinal sill (CS in fig. 1), the velocity of the flows is proportional to $g'^{1/2}$, g' being the reduced gravity defined as $g' = g\ (\rho_2 - \rho_1)\ /\rho_0 = g\ \Delta\rho\ /\rho_0$, where ρ is the density and subscripts 1 and 2 refer to the Atlantic and

Mediterranean layers respectively (Farmer and Armi, 1986; Bormans et al., 1986; Bryden et al., 1994; García-Lafuente et al., 2002). In a real stratified model, the relationship between u and $\Delta\rho$ remains and, thus, the seasonality of the transport depends on the seasonality of h and $\Delta\rho$.

The Mediterranean outflow is mainly composed of Levantine Intermediate Water (LIW) and, to a lesser extent, of Western Mediterranean Deep Water (WMDW). Millot et al. (2006) also showed contributions of Tyrrhenian Deep Water (TDW) and Western Intermediate Water (WIW). The properties and fractions of these waters at Espartel sill (ES in fig. 1), together with some traces of North Atlantic Central Water (NACW) present in the Mediterranean vein through mixing with the upper layer, determine the thermohaline characteristics of the waters leaving the strait. The proportion of WMDW in the outflow depends on the capacity of the flow to aspirate deep water from the Alboran Sea by Venturi-Bernouilli effect, a mechanism that can uplift waters from 600-700 m depth and incorporate them to the outflow (Stommel et al., 1973; Kinder and Bryden, 1990). This is favoured when the winter deep convection in the Gulf of Lions reaches the bottom, filling it with newly formed WMDW and uplifting the ancient that is now available to be suctioned out through Gibraltar more easily. Other factors, like the circulation pattern in the Alboran Sea and the meteorological forcing also contribute to the process, varying the amount of deep water available (García-Lafuente et al., 2009, Naranjo et al., 2012).

The final properties of the Mediterranean waters leaving the strait are the result of a complex mixing process driven by tides, internal waves and the topographical constrains (García-Lafuente et al., 2011; Sannino et al., 2009). The Strait of Gibraltar is known as the key controlling factor of the Mediterranean Sea circulation in ocean regional circulation models since a long time (Bryden and Stommel, 1984; Artale et al.

2006). Many authors evaluated or studied this specific location in models, either through case studies (Vlassenko et al., 2009; Sánchez-Garrido et al., 2011), longer hindcast runs (Béranger et al., 2005; Tonani et al., 2008; Sannino et al., 2009; Oddo et al. 2009) or in regional climate change scenarios (Thorpe and Bigg, 2000; Somot et al., 2006). However, up to now and to our knowledge, no research on the evaluation of the climate variability of long-term hindcast simulations against long-term in-situ observations has been carried out. Indeed long time series of in-situ observations have been completed only recently (Soto-Navarro et al. 2010). The main goals of the paper are (1) to show how in-situ observations can help evaluating climate-scale ocean models at the Strait of Gibraltar, (2) to evaluate state-of-the-art ocean regional circulation models at the Strait of Gibraltar for climate-scale variability (mean behaviour, seasonal cycle), (3) to identify some of the key factors explaining the model skills in using an ensemble of simulations and (4) to list some ideas for model improvements.. The paper mainly relies on the observations collected in the Espartel Sill and described in Soto-Navarro et al. (2010) and on multi-annual simulations performed with different configurations of the Mediterranean Sea based on the numerical model NEMO (Madec et al. 2008). Due to the characteristics of the data the comparison will be focused in the volume transport and the thermohaline properties of the Mediterranean outflow. We describe the observations in section 2 and the models and simulations in section 3. Model evaluation is performed in section 4 for the mean behavior and the seasonal cycle before establishing the conclusions in section 5.

2 Observations

The Strait of Gibraltar is a system of sills and narrows about 60 km long and 20 km wide, with a minimum width of less than 14 km in the Tarifa narrow section (TN) and a minimum depth of 290 m in the Camarinal sill (CS), located west of Tarifa (fig.

1). The observational data have been collected by a monitoring station in the Espartel sill (ES). The station was first deployed in September 2004 at the southern and main channel of the sill (35º51.7’ N, 5º58.6’W), at 356 m depth and is still acquiring information. It was equipped with an up-looking 75 kHz Acoustic Doppler Current Profiler (ADCP) 20 m above the seafloor that provides 3-D velocity in 8-m thick bins every 30 minutes up to a depth above the Mediterranean-Atlantic interface layer, whose mean depth in Espartel is around 190 m (Sánchez-Román et al., 2009). Below the ADCP, at 10 m above the seafloor a Conductivity Temperature (CT) probe samples the conductivity and temperature of the Mediterranean water. The station is completed by a point wise current meter settled between the CT and the ADCP to measure the velocity in the shadow area of the ADCP allowing the full sampling of the Mediterranean vein velocity.

The Mediterranean outflow is computed from the velocity according to

$$Q_2(t)=\int_{b}^{h(t)}\langle u(z,t)\rangle W(z)\,dz \qquad (1)$$

where $\langle u(z,t)\rangle$ is the along-strait velocity, previously filtered to remove tidal and subinertial variability (periods lower than 21 days); *W(z)* is the channel width at depth *z* and *h(t)* is the time-dependent depth of the surface of zero low-passed velocity (interface). This transport computation presents two inconveniences: it has implicitly assumed that the single velocity profile at ES is representative of the entire channel section ignoring the cross-channel structure of the flow. Moreover, only the southern main channel of the Espartel section is considered (south of Majuan Bank, MB in figure 1), so Mediterranean water outflowing through the small, secondary northern channel is neglected. Sánchez-Román et al. (2009) used an improved version of the CEPOM numerical model developed by the Ocean Modelling Unit of ENEA to complement the observations and correct the flow estimations. Model outputs provide information to assess the accuracy of the outflow estimations from observations at a single station and shows that when the cross-strait structure of the velocity field is taken into account the flow computed from a single station must be reduced around 22% due to lateral friction. The model also indicates that the fraction of the outflow through the northern channel of ES is around 18% of the total outflow. Both corrections have been incorporated to outflow estimations in (Eq. 1).

3. Models and Simulations

Three Mediterranean configurations based on the NEMO code (Madec et al. 2008) are used in this study: NEMOMED8, NEMOMED12, and NEMOMED36. They differ essentially by their grid resolution and are currently being used in climatic studies of the Mediterranean circulation. One of the aims of this work is to investigate whether these configurations give rise to a good representation of the exchange in the strait, and hence can be helpful in the interpretation and analysis of the results for the rest of the basin. The model grids cover the whole Mediterranean and a buffer zone including a part of the Atlantic Ocean. The following subsections describe the model configurations, their parameterizations and their atmospheric forcing and freshwater inputs.

3.1 Model configurations

NEMOMED8

The NEMOMED8 model (Sevault et al., 2009; Beuvier et al., 2010; Herrmann et al., 2010) has been developed from previous works done with OPAMED8 (Somot et al., 2006), which was a coarse companion configuration of OPAMED16 (Béranger et al., 2005; Drillet et al., 2005). The horizontal resolution is 1/8º x 1/8º cos(φ), with φ the latitude, equivalent to a range of 9 to 12 km from the north to the south of the Mediterranean domain. NEMOMED8 is considered as an eddy-permitting model according to a mean deformation radius of 10 km in the Mediterranean Sea. As for OPAMED16, the originality of the NEMOMED8 grid is its tilt and stretch at the Strait of Gibraltar, built in order to match its SW-NE axis, hence the resolution increases locally to 6 km in the strait (two grid points in the narrowest section). NEMOMED8 has 43 vertical Z levels, with an inhomogeneous distribution (from ΔZ=6 m at the surface to ΔZ=200 m at the bottom with 25 levels in the first 1000 m). The bathymetry is based on ETOPO 5'x5' database (Smith and Sandwell, 1997).

NEMOMED12

NEMOMED12 (Lebeaupin Brossier et al. 2011, 2012; Beuvier et al. 2012) is a higher resolution configuration, which uses the standard ORCA grid of NEMO at 1/12º resolution. This corresponds in the Mediterranean area to a grid cell size between 6 and 8 km, from 46ºN to 30ºN. The NEMOMED12 model is also considered as eddy-permitting. The bathymetry is not particularly stretched at the strait of Gibraltar. It has 50 vertical stretched levels (from ΔZ=1 m at the surface to ΔZ=450 m at the bottom with 35 levels in the first 1000 m). The bathymetry comes from the 10th MERCATOR-LEGOS bathymetry at 30"x 30" resolution, composed of merging between the GEBCO-0.8 database, the MEDIMAP bathymetry (Medimap Group, 2005) and the Ifremer bathymetry of the Gulf of Lions (Berné et al., 2004).

NEMOMED36

NEMOMED36 is the companion configuration of NEMOMED12 and the higher resolution product of the NEMOMED models hierarchy (Beuvier, 2011). Its horizontal grid is based on the standard ORCA grid of NEMO at 1/36° resolution (3 times the NEMOMED12 grid). This corresponds in the Mediterranean area to a grid cell size between 2 and 3 km, from North to South. The NEMOMED36 model is also considered as eddy-permitting. The configuration used has the same 50 vertical levels of NEMOMED12 and the same bathymetry MERCATOR-LEGOS has been interpolated on its grid.

3.2 Parameterizations

The main parameters of the simulations are summarized in Tables 1 and 2. All the configurations use very similar parameterizations. To fit the real bathymetry, a partial cell parameterization is used, i.e. the local deepest level in the model has variable depth. The horizontal eddy diffusivity is applied with a Laplacian operator and the horizontal viscosity coefficient for the dynamics (velocity) is applied with a bi-harmonic operator. A 1.5 turbulent closure scheme is used for the vertical eddy diffusivity (Blanke and Delecluse, 1993) with an enhancement of the vertical diffusivity coefficient in case of unstable stratification. The Total Variance Dissipation (TVD) scheme is used for the tracer advection and the EEN (Energy and ENstrophy conservative) scheme is used for the momentum advection (Arakawa and Lamb, 1981; Barnier et al., 2006). The solar radiation can penetrate into the ocean surface layer (Bozec et al., 2008). A no-slip lateral boundary condition is used and the bottom friction is quadratic. The evolution of the sea surface is parameterized by a filtered free surface (Roullet and Madec, 2000).

Exchange with the Atlantic Ocean

The exchange with the Atlantic Ocean is performed through a buffer zone. From 11ºW to 7.5ºW, 3D temperature and salinity of the model are relaxed towards T-S climatological fields. This relaxation is a Newtonian damping term in the tracer equation, equal to -($X_{model} – X_{climatology}$)/$\tau$. The restoring term is weak west of Cádiz and Gibraltar area (τ = 100 days for NM8, 90 days for NM12/36 at 7.5ºW) and stronger moving westward (τ = 3 days for NM8, 2 days for NM12/36 at 11ºW). The climatologies used in the buffer zone for the different simulations are summarized in Table 1. For NEMOMED8, monthly anomalies computed on the data mean (1960-2005) from Daget et al. (2009) are added to the Reynaud climatology (Reynaud et al. 1998). For NEMOMED12 and NEMOMED36, 3D temperature and salinity of the model are relaxed towards the T-S climatological fields of Levitus et al. (2005).

Volume conservation

Two different methods are used in order to assure the model volume conservation in the whole domain (Mediterranean Sea + Atlantic buffer zone), a high constraint considering that the Mediterranean Sea evaporates about 700 mm/year (Mariotti et al., 2002; Criado-Aldeanueva et al., 2012).

In the first method the water volume corresponding to the net evaporation averaged over the Mediterranean Sea is added as precipitation at each time step over the Atlantic area, between 11°W and 7.5°W (Tonani et al. 2008; Beuvier et al. 2010).

In the second method (Beuvier et al. 2012) the Sea Surface Height (SSH) of the model is relaxed towards a climatological SSH obtained from a global simulation. In this case GLORYS1V1 reanalysis (Ferry et al. 2010), a reanalysis of the global ocean circulation at 1/4º horizontal resolution available for the 2002-2008 period, has been used. As a result the exchange at Gibraltar is forced by the sea level difference between the Atlantic and Mediterranean. It implies that the net transport through the Strait of Gibraltar is not anymore equal to the Mediterranean Sea E-P-R (Evaporation minus

Precipitation and Runoff) budget as it was by construction in the first method. Apart from conserving the model volume, the SSH relaxation in the Atlantic buffer zone allows the model to correctly represent the SSH on the Mediterranean. GLORYS1V1 reanalysis uses the AVISO Sea Level Anomaly as an assimilated data.

Bottom friction

The bottom friction, F, is parameterized as:

$$\vec{F} = C_D \sqrt{U_H^2 + V_H^2 + E}\,\vec{U}_H \quad (2)$$

where C_D is the drag coefficient, U_H and V_H the zonal and meridional velocities of the bottom layer respectively, $\vec{U}_H$ the horizontal bottom velocity vector and E is the bottom turbulent kinetic energy background. For the latter two different schemes have been used (Table 2): a constant value or a 2D field that incorporates the mean tidal energy computed by the tidal model of Lyard et al. (2006). The mean tidal energy is the highest at the Strait of Gibraltar (maximum value over 10000 cm^2s^{-2}) and has significant values mainly in the Channel of Sicily, in the Gulf of Gabes and in the northern Adriatic Sea.

3.3 Surface boundary conditions

River runoff and Black Sea

The freshwater flux due to rivers runoff is explicitly added to complete the water budget. In the NEMOMED8 simulations, a monthly runoff is added at the main 33 river mouths of the Mediterranean, computed as a combination of the RivDis Database climatology (Vörösmarty et al, 1996) and the interannual variations coming from Ludwig et al. (2009). In NEMOMED12 and NEMOMED36 the values of the inputs of the other rivers are gathered and averaged in each Mediterranean sub-basin (as defined in Ludwig et al. (2009)) and put as a coastal runoff in each coastal grid point of these subbasins.

The Black Sea, not included in the models, is one of the major freshwater sources of the Mediterranean Sea. The exchanges between the Black Sea and the Aegean subbasin consist in a two-layer flow across the Marmara Sea and the Turkish strait (Oguz and Sur, 1989). This exchange is replaced by a net freshwater flux diluting the salinity of the mouth grid point. Thus, the Black Sea is considered as a river for the Aegean Sea. In the simulations, monthly values are derived from Stanev et al. (2000) and Stanev and Peneva (2002). Note that the rivers and Black Sea runoffs are the same as in Beuvier et al. (2010).

ARPERA atmospheric forcing

ARPERA high resolution atmospheric data are used for the air-sea fluxes. ARPERA is obtained by performing a dynamical downscaling of the ERA40 reanalysis (resolution 125 km) from the European Centre for Medium range Weather Forecast (ECMWF, Simmons and Gibson, 2000) up to 2001 and of the ECMWF analysis downgraded to the ERA40 resolution from 2002. It means that a break is possible in 2001 even if the RCM ARPEGE is the same for the whole period. The downscaling method is described in Guldberg et al. (2005). The principle is to use a global stretched-grid atmospheric model, here ARPEGE-Climate, allowing reaching a 50 km resolution over the Mediterranean Sea (Déqué and Piedelievre, 1995), in which small scales can develop freely and large scales are driven by the ECWMF reanalysis. The synoptic chronology then follows that of ECMWF while the high-resolution structures of the atmospheric flow are created by the model. All details can be found in Herrmann and Somot (2008), Tsimplis et al. (2009) and Beuvier et al. (2010).

Daily mean fields of momentum, freshwater flux (evaporation minus precipitation) and net heat flux (mean sea level pressure is not used to force the models) are used to force the ocean. The heat flux is applied with relaxation term using the ERA-40 Sea Surface Temperature (SST). This term plays actually the role of a first order coupling between SST of the ocean model and the atmospheric heat flux, ensuring the consistency between those terms (Barnier et al., 1995). Following the CLIPPER Project Team (1999), the relaxation coefficient is -40 $Wm^{-2}K^{-1}$, which is equivalent to 8 days restoring time scale. Then the surface fresh water budget is balanced adding a monthly correction term designed as in Beuvier at al. (2010). No salinity damping is used at the surface.

ECMWF atmospheric forcing

ECMWF reanalysis is applied using the CLIO bulk formulation (Goosse et al. 2001), which allows to compute the heat and water fluxes from the atmospheric variables. In addition to the ECMWF forcing, a Sea Surface Salinity (SSS) restoring is applied with a damping coefficient of -16.7 mm/day, towards the monthly SSS climatology.

3.4 Simulations

The set of simulations and their main characteristics described in the following are summarized in tables 1 and 2.

NM8 simulations

Two different simulations based in NEMOMED8 are presented in this work. The first one, NM8-NOSSH hereinafter, covers the period 1961-2010 after 15 years of spin-up. To assure the model volume conservation in NM8-NOSSH, the net evaporation on the Mediterranean is added as precipitation in the Atlantic zone at each time step.

The second simulation, NM8 hereinafter, covers the 2002-2008 period. The model volume is conserved through a damping of the Sea Surface Height (SSH). The NM8 begins from the restart of NM8-NOSSH in August 2002.

NM12 simulations

Four different simulations based on NEMOMED12 are presented in the following and cover the 2002-2008 after 3 years of spin-up. Three of them are forced by ARPERA and the last one is forced by ECMWF.

For the first one, NM12-ARP hereinafter, the net evaporation on the Mediterranean is added as precipitation in the Atlantic zone at each time step and the bottom friction is set to constant (*E = CST).*

For the second one, NM12-ARP-2DE hereinafter, the net evaporation on the Mediterranean is added as precipitation in the Atlantic zone at each time step and the bottom friction used a 2D field for *E* that takes into account the mean tidal kinetic energy dissipation. It is the same as NM12-ARP except for *E*.

For the third one, NM12 hereinafter, the model volume is conserved through a damping of the Sea Surface Height (SSH) and the bottom friction used a 2D field for E. It is the same as NM12-ARP-2DE except for the SSH damping in the Atlantic area.

For the fourth one, NM12-ECMWF hereinafter, the net evaporation on the Mediterranean is added as precipitation in the Atlantic zone at each time step and the bottom friction used a 2D field for E. It is the same as NM12-ARP-2DE except for the atmospheric forcing.

NM36 simulation

The simulation from NEMOMED36, NM36 hereinafter, covers the period from the 1st August 2003 to the fall of 2007. It starts with an ocean at rest and from the averaged August 2003 θ and S fields of its NM12-ECMWF companion simulation. It is also forced by the ECMWF analyses.

To sum up, the analysis will be focused on the model resolution, the atmospheric forcing, the parameterization of the Atlantic buffer zone and the bottom friction scheme, which constitute the main differences between the set of simulation described (tables 1, 2).

4. Model comparison

The evaluation process has been focused on two topics: the seasonality of the volume transport and the thermohaline characteristics of the outflowing waters. For the first one we have analyzed the inflow, outflow and net flow seasonal cycles, focusing on the outflow, for which direct measurements are available. The inflow and net flow have been compared with the indirect estimations of Soto-Navarro et al. (2010, SN10 hereinafter), based on a combination of reanalysis, model and observed data. The transport has been computed across different sections for the models and for the observations, Tarifa and Espartel sections respectively (fig. 1). At seasonal time scale, the differences between these two sections due to entrainment are not higher than 3% (García-Lafuente et al., 2011), in any case smaller than the standard deviation of the monthly time series used in the comparison.

The evaluation of the outflow θ-S characteristics have been performed comparing the model outputs with the observations at the grid points closest to the

Espartel station (table 2). Both the water thermohaline characteristics and the fraction of LIW, WMDW and NACW composing the flow have been analyzed. Because of the availability of observational data, the comparisons are established from 2004.

4.1 Volume transport

The monthly mean time series of the outflow for the observations and simulations after 2004 are represented in figure 2a. NEMOMED8 simulations show better agreement with the observations, particularly NM8-NOSSH in the last two years 2008 and 2009. Table 4 also reflects this fact, with higher correlation for NEMOMED8 and lower for NEMMOMED12 simulations and NM36. In terms of mean values, NM8 and the observations almost coincide for the outflow and inflow (table 5) while in NEMOMED12 simulations and NM36 both flows are underestimated. The mean net flow is very similar for all the simulations and close to SN10. It is important to notice that the mean flows are almost the same among all NEMOMED12 simulations, and the highest discrepancy is found for NM36, with an underestimation of 19% for the outflow and 16% for the inflow.

The outflow seasonal cycle is also better represented by NEMOMED8, especially by the simulation including SSH relaxation in the Atlantic buffer zone, NM8 (green line, fig. 2b). The cycle of both NM8 simulations is included in the variability range of the observations. The maximum in April, likely linked with the winter WMDW production in the Gulf of Lions (Sánchez-Román et al., 2009; Soto-Navarro et al., 2010), is very well captured by both simulations. On the other hand, the transport in spring and summer is overestimated. Reinforcing this result, the 12-month correlation of the seasonal cycle is very high for NEMOMED8 simulations, with values of 0.71 and 0.75 (table 4). For NM12 and NM36, the seasonality is not so well represented and the

12-month correlation is lower: between 0.57 and 030 for NEMOMED12 and 0.64 for NM36. The seasonal cycles of these simulations are very similar, showing the spring maximum one month delayed respect to the observations, and their evolution in the last months of the year is very different to the observed one.

The net flow seasonality reflects the net surface water flux (E-P-R-B) seasonal cycle (same as the net flow in NM8-NOSSH, blue line in fig. 2c), although some differences are achieved when the SSH variability in the Atlantic is considered (fig. 2c). In the simulations that include SSH relaxation, the net flow is driven by the sea level difference between the Atlantic and the Alboran Sea, while when the SSH relaxation is not included the net flow is the result of the artificial incorporation of the net evaporation over the Mediterranean basin as precipitation in the Atlantic. The first and more realistic mechanism produces better results, with a more pronounced decrease in late autumn that agrees better with SN10. For instance, in the cycle of NM8 (green line in fig. 2c) the maximum in late summer and the minimum in April coincide with the results of SN10, while for NM8-NOSSH (blue line in fig. 2c) the maximum occurs in November and the minimum is shifted to May. The last two rows in table 5 show that the mean values of the net flow and the water deficit are very close for all simulations. The SSH variability only affects the shape of the cycle so in the long-term the net flow must compensate the net evaporation losses of the basin and the SSH damping do not influence the mean value. Furthermore, the ECMWF dataset used as atmospheric forcing in NM36 and NM12-ECMWF provides mean net evaporation similar to ARPERA.

In the seasonality of the inflow (fig. 2d), the positive effect of the SSH damping to achieve a realistic representation is evident for NEMOMED8. Although the net flow cycle is very similar for the two simulations (fig. 2c), the one including this mechanism shows much better results for the inflow than the one which do not include it when comparing with SN10 estimation. Indeed, NM8 shows very high 12-month correlation with the seasonal cycle of SN10, 0.88, while NM8-NOSSH has a low 0.57. NM12 and NM12-ARP-2DE also show higher correlation than NM12-ARP (0.80, 0.72 and 0.68 respectively). Except for NM8-NOSSH (for which the shape of the seasonal cycle is completely different than SN10 and the rest of simulations) the summer maximum coincides in the cycle of both net flow and inflow, but in NM8 (green line in fig. 2d), the inflow shows a secondary maximum in spring that is not appreciated in SN10 and may be a consequence of a velocity increase due to the outflow maximum in this season.

The results of the previous analysis point out the small differences between the four simulations based on NEMOMED12. They show almost the same mean values for both components of the flow and their seasonal cycles are very close. Only NM12-ECMWF (light blue line in fig. 2) has a slightly different seasonality, which can be attributed to the differences in the Mediterranean Water Budgets (MWB) of ARPERA and ECMWF datasets. These differences are around 15% in their common period, in good agreement with the climatological estimations of Mariotti (2011), although the influence in the volume transport is very low (~1% for inflow and outflow). Furthermore, the comparison between NM12-ARP and NM12-ARP-2DE shows that the effect of the 2D E field in the bottom friction parameterization is negligible, without any noticeable influence in the volume transport. The bottom friction can then be locally enhanced by the introduction of the 2D field, but it does not have the same effect as that indicated by Dussin and Treguier (2010), who doubled the C_D coefficient keeping E constant. For these reasons, in the following the NEMOMED12 analysis will focus only in NM12 simulation, which achieves the better results for the volume transport (tables 4 and 5).

A possible explanation of the underestimation in the mean values for both inflow and outflow in NM12 and NM36 could be a too low velocity of the flow, especially in the Mediterranean layer. Figure 3a shows that the velocity profiles at ES of NM12 and NM36 are more realistic, with the maximum at the center of the Mediterranean layer, although the velocity is lower than the observed along the whole water column. In contrast NM8 overestimates the velocity of the upper layer and reaches the maximum at the bottom level. The possible effect of the bottom friction parameterization to explain these differences is discarded from the analysis of NM12-ARP and NM12-ARP-2DE simulations. On the other hand the analysis of NM12-ECMWF and NM36 companion simulations show an important impact of the model resolution in the mean values of the flow components, with a reduction of ~10%. Considering that both configurations use no-slip boundary condition, since in NM36 the geometry of the strait and its shelf are more precisely described (fig. 1c, d) the interaction between the bathymetry and the current is stronger and the flow can be slowed down by roughness effect. This transport decrease as a result of the resolution increase and the use of no-slip boundary condition and quadratic bottom friction (proportional to the bottom speed) seem to be in agreement with the results of Dousin and Treguier (2010). The same hypothesis can be applied to explain the higher velocities of NM8. Although the resolutions of NM12 and NM8 are similar in the strait area, that is not the case in the rest of the domain, so an increase of the NM8 velocity with respect to NM12 could be also an effect of the flow-bathymetry interaction.

Another factor to be considered is the density difference between the Mediterranean and Atlantic layers. As pointed out in section 1, the velocity of the flows depends on $\Delta\rho$. Since the Mediterranean layer has a rather steady density, the seasonal cycle of $\Delta\rho$ follows the changes in the density of the Atlantic layer, which is mirrored by the sea level seasonal cycle whose origin is the thermal expansion of the water column (steric effect). Figure 3b shows $\Delta\rho$ seasonal cycle for all the simulations at the Tarifa section, computed as the difference between the integrated density for the layers of negative and positive velocities. The mean values range between 2.2 $kg \cdot m^{-3}$ and 2.3 $kg \cdot m^{-3}$ so there are not important differences between the models and simulations studied, even when different datasets are used as atmospheric forcing or in the Atlantic area for each one. The maximum values in late summer coincide with the maximum of the temperature seasonal cycle (Cazenave et al., 2002; Criado-Aldeanueva et al., 2008) and reinforces the maximum in the inflow (fig. 2d). Therefore, the lower velocity of the flow for NM12 and NM36 is not consequence of the different forcing applied on each simulation.

In addition to the velocity of the flow, *u*, the second variable controlling the volume transport is the depth of the interface between the Mediterranean and Atlantic layers, *h* (Eq. 1). Taking into account the differences in the depth of the sill for the three models (table 3), all simulations show a very good agreement with the observations in the mean value of the interface depth, around 55% of the water column at the sill (fig. 3c). The shape of the seasonal cycles is also fairly well reproduced, with a minimum depth coinciding with the maximum outflow in spring (fig. 2b), although for NM36 the cycle is too flat, with very small amplitude between the spring minimum and the winter maximum. The interface depth seasonality is mainly forced by the water deficit and thus its cycle and the net flow cycle are very similar (compare fig. 2c and 3c). Besides, another factor affecting the interface variability is the volume of WMDW present in the adjacent basin, the Alboran Sea, which could contribute to the minimum depth in spring by raising the interface between the LIW and WMDW after the winter convection process in the Gulf of Lions, and then also raising the Mediterranean-Atlantic interface (Soto-Navarro et al., 2010). The one month shift of the minimum in the models may be a consequence of an underestimation of the deep water volume formed that leads to a slower rising of the interface in the Alboran Sea. Other possibilities are a time shift in this process (too early or too late in the model) and/or a too weak propagation phase of the newly formed dense water. For this last point, it should be noted that NM8 and NM12 are not fully eddy-resolving and, as the propagation phase is partly due to small eddies advecting the newly formed dense water, this could also influence the seasonality of the interface (Herrmann et al., 2011; Beuvier et al., 2012). .

To summarize, in spite of the different atmospheric or Atlantic forcing used in the simulations, $\Delta\rho$ and h are very similar among all of them. The small differences in the transport between the four NEMOMED12 simulations reinforce this result. A stronger roughness effect in NM12 and NM36, slowing down the current due to the flow-bathymetry interaction as a consequence of their higher resolution, seems to be responsible of the better results achieved by NM8. It is worth to point out the positive effect of the use of SSH damping in the Atlantic buffer zone, which leads to a much more realistic representation of the seasonality of the volume exchange.

4.2 Thermohaline characteristics of the outflow

In the θ-S diagram of figure 4a, the ES observations and the different simulations in their common period are represented. The NM8-NOSSH and NM8 show similar values, with abnormally warm waters. We recall that NM8 starts from NM8-NOSSH and consequently inherited from NM8-NOSSH biases. One explanation to the bias could lie in the abnormally high temperature and salinity of the intermediate layer in the western basin that make LIW be warmer and saltier than in the observations (Beuvier et al., 2010). In contrast, the outflow properties in NM36 and, particularly, in NM12 fit well the observations, this meaning that both the properties of the different water masses in the Mediterranean basin and their eventual proportion in the outflow composition are better represented.

The other factor controlling the thermohaline characteristics of the outflow is the fraction of the different water masses that it comprises. Figures 4b, c show these fractions for observations and simulations respectively. The characteristics of the LIW and WMDW in the Alboran Sea, and those of the NACW in the Gulf of Cádiz, have been used as a reference for the estimations. For the observations the reference θ-S values have been retrieved from previous works based on oceanographic surveys (Parrilla et al., 1986; MEDAR Group, 2002), and are summarized in table 6 (the points for the reference values of the LIW and WMDW are represented by black stars in the θ-S diagram of fig. 4a, the NACW point is out of the diagram). For the simulations, the θ-S pairs have been computed every year, using the values corresponding to the maximum salinity of the spatially averaged vertical profile in the Alboran Sea for the LIW and to the minimum temperature for the WMDW. For the NACW the mean values at 150 m depth (approximately the depth of the interface between inflow and outflow) in the Gulf of Cádiz have been used. This procedure aims to take into account the interannual to long-term variability of the salinity and temperature in the models for the intermediate and deep layers (Beuvier et al., 2010), redefining the water masses characteristics according to those of the simulations (table 6). Of course this should be considered as an approximation. The hydrological properties of the water masses are variable in time and space over the strait area. This decomposition has been performed in order to compare the outflow composition of the models and the observations, and not to describe it with accuracy. The approach used for the observations may affect, for example, the interannual variability or the trends in the water mass fractions, introducing spurious values, since the water masses properties used as reference are constant in time.

The results show that the fraction of the WMDW is clearly underestimated in NM8, this making the outflow be almost completely composed by LIW and, thus, warmer. It is also important to notice that the fraction of NACW in these simulations is around 0.09, slightly higher than the 0.05 of the observations. Even though these values are close, the great difference between the properties of NACW and Mediterranean waters makes this discrepancy have an important effect in the θ-S characteristics of the resulting mixed waters that leave the strait. A factor to be considered for the higher mixing ratio of NM8 is the numerical vertical diffusion, higher in this model due to its lower resolution, which probably has some influence in its worst performance. For NM12 the outflow composition is very close to the observed data, with a mean fraction of 0.65 for LIW (0.59 in observations), 0.33 for WMDW (0.36 in observations) and 0.03 for NACW (0.05 in observations). For NM36 there is a good agreement in the first two years but not from 2006 onwards, when a strong drift is observed, increasing the fraction of LIW up to 1. This drifting could be a consequence of the short period simulated.

The main driving force for the aspiration of WMDW is tides (Kinder and Bryden, 1990). Since they are not included in the models, the low fraction of WMDW, and hence the overestimation of the amount of LIW is not unexpected, but there is a clear difference among the three models. In NM8 the proportion of the water masses is highly biased, although the recent years of large deep water formation, for instance 2005, 2006, 2009 and 2010 (López-Jurado et al., 2005; Schroeder et al., 2008; Loïc

Houpert, CEFREM, pers. comm.), are reflected in all simulations with an increase in the proportion of WMDW (a mean value of 0.15 in 2005 in contrast with 0 in 2007 and 2008). For NM12 and NM36 the composition of the flow is much closer to the observations. The main reason for this difference is the depth at which the WMDW is found in the Alboran Sea for the different models. In fig. 5 the cross sections of temperature at 4ºW and 6ºW for the three models are represented. For NM8 the coldest waters east of the strait are found deeper than 1000 m (fig. 5a), a depth that make them inaccessible to be suctioned over the sill. In contrast, for NM12 and NM36 (fig. 5b, c) the coldest waters can be found up to 600-700 m. From this depth the deep waters are more suitable to be aspirated and incorporated to the outflow. Moreover, the higher resolution of NM12 and NM36 leads to a better representation of the mesoscale features in the adjacent basin that may affect the ventilation process. Naranjo et al. (2012) argue that the Western Alboran Gyre (WAG) helps to accumulate dense water in the eastern approach of the strait, which makes it available for its subsequent aspiration. Therefore, the ability of the higher resolution models to realistically resolve the WAG may have improved their capacity to reproduce the WMDW aspiration and hence its proportion in the outflow. However, this potentially interesting link is a hypothesis that requires further study to be proved.

West of Gibraltar the waters masses distribution of the three simulations is very similar (fig. 5d, e, f). The Mediterranean Outflow Waters (MOW) resulting from the mixing at the strait (warmer than the Mediterranean waters at the Alboran Sea) flows into the Atlantic mainly through the southern channel (Sánchez-Garrido et al., 2009), below the NACW and the surface waters. In NM12 and NM36, the waters at 150 m (the depth of the Mediterranean-Atlantic interface at the strait) are warmer; however the resulting MOW are closer to the observed ones, this reinforcing the better behaviour of these models in the representation of the mixing processes.

To further investigate the influence of the fraction of each different water mass in the final θ-S properties of the outflow, three tests were performed for NM8, imposing different conditions to the outflow composition while the characteristics of the water masses were kept constant (with the same values used in the decomposition)(fig. 4d). Grey points in fig. 4d are the resulting θ-S values when the fraction of NACW is forced to be 0.05, purple points are the values obtained when WMDW fraction is set to 0.35 and orange points result when both previous conditions are imposed at the same time (these values have been chosen following the results of the observations at ES, fig. 4b). The red and blue circles represent the positions of the ES data and the original NM8 points, respectively. All tests imply significant changes, with the resulting mixed waters closer to the observations, although a good parameterization of the mixing with the NACW seems to be more important. Indeed, the great difference between the characteristics of the Atlantic and Mediterranean waters makes a small variation in their mixing ratio have a large impact in the outflow properties.

To sum up, the properties of the Mediterranean waters are well reproduced in NM36 and especially NM12. Due to their higher resolution, the physical processes in the basin are probably better resolved and consequently the salinity, temperature and the fraction of the different water masses present in the outflow are closer to the observations. Despite this good agreement, it must be noted that the MOW is the result of complex mixing processes along the strait, especially at Camarinal sill, that are not specifically incorporated in the models by parameterization. In NM8 the bias in the LIW temperature, the difficulty to incorporate WMDW to the flow and the higher amount of NACW results in too warm Mediterranean water.

5. Summary and conclusions

A set of simulations from NEMOMED8, NEMOMED12 and NEMOMED36 regional circulation models of the Mediterranean Sea have been compared with observations collected at the Espartel station in order to evaluate their representation of the exchange through the Strait of Gibraltar in terms of volume transport and thermohaline properties of the Mediterranean outflow.

NM8 shows better results for the volume transport, with mean values very close to the observations, and seasonal cycles varying within the range of the observed ones for both inflow and outflow. In NM12 and NM36 the inflow and outflow mean values are underestimated, although the seasonal cycles are quite similar to NM8. The reason for this underestimation is a too low velocity of the flow, which could be a consequence of the flow-bathymetry interaction, which is stronger in NM12 and NM36 due to their higher resolution, this slowing down the flow by roughness effect. On the other hand, the different datasets used as atmospheric forcing and in the parameterization of the Atlantic buffer zone do not have any remarkable effect in the density difference between the inflow and outflow layers, and hence in the velocity of the flow. In addition, the depth of the interface between these layers, the second variable controlling the exchange, is not affected either. Indeed, the analysis of the set of NEMOMED12-based simulations shows that the different atmospheric forcings (ECMWF or ARPERA) and parameterizations (constant or 2D *E* field) do not have any remarkable effect in the volume transport.

An important improvement in the representation of the exchange seasonality is achieved by the simulations including SSH variability of the Atlantic buffer zone. For the net flow and especially for the inflow, the seasonal cycle is much better described by the simulation including this element, as expected considering that it implies a more realistic mechanism driving the exchange.

The Mediterranean outflow waters are warmer and slightly saltier in NM8 due to three main causes: the first one is a too warm LIW; the second is the small fraction of WMDW in the flow consequence of the too deep pooling of this water mass in the Alboran Sea. Finally, the high percentage of NACW in the flow, which is almost double than in the observations and have a strong impact in the salinity and temperature of the outflow due the large difference between the Atlantic and Mediterranean water properties. In contrast, in NM36 and especially in NM12 the outflow properties and its composition fit quite well the observations. The LIW and WMDW thermohaline properties in these simulations are closer to the observed ones, and the higher resolution of NEMOMED12/36 leads to a better representation of the physical processes in the whole basin. As a result, the position of the water masses in the Alboran basin, local dynamical features as the western Alboran gyre and mechanisms as the deep water aspiration in the Strait sill are better resolved, all these contributing to the good results of NM36 and NM12.

Among the studied models, the most suitable to achieve an accurate representation of the exchange through the Strait of Gibraltar are those of higher resolution (NM12 or preferably NM36). These configurations perform a better representation of the thermohaline properties of the outflow, although further investigation is needed to clearly understand the differences in volume transport. However, due to the complexity of the exchange through the Strait of Gibraltar, even NM36 is not able to fully represent the physical processes involved and needs the inclusion of *ad hoc* parameterization in this area. The extension of the in situ time series will make possible forthcoming studies focused on the interannual variability and trends analysis that this work is lacking. Furthermore, an intercomparison with other models not based in NEMO would be very worthy in order to test the consistence of the obtained results, perhaps in the framework of international coordinated projects as HyMex (www.hymex.org) or Med-CORDEX (www.medcordex.eu). The study of the possible evolution of the Mediterranean waters and the exchange characteristics in climate change scenarios would also be an interesting future line.

Acknowledgments

This work has been carried out in the frame of the P07-RNM-02938 Junta de Andalucía (JA) Spanish-funded project. Partial support from CTM2010-21229/MAR (INGRES 3) is also acknowledged. The main part of the work was developed during a research stay at Météo-France/CNRS, CNRM-GAME group, in Toulouse (France), funded by JA.

References

Arakawa, A., and V. R. Lamb (1981), A Potential Energy and Enstrophy Conserving Scheme for the Shallow Water Equations, *Mon. Weather Rev.*, 109, 18–36.

Artale V., Calmanti S., Malanotte-Rizzoli P., Pisacane G., Rupolo V., Tsimplis, M. (2006) Chapter 5 The Atlantic and Mediterranean Sea as connected systems, In: P. Lionello, P. Malanotte-Rizzoli and R. Boscolo, Editor(s), Developments in Earth and Environmental Sciences, Elsevier, 2006, Volume 4, Pages 283-323, ISSN 1571-9197, ISBN 9780444521705, 10.1016/S1571-9197(06)80008-X.

Barnier, B., L. Siefridt, and P. Marchesiello (1995), Thermal forcing for a global ocean circulation model using a three-year climatology of ECMWF analyses. *J. Marine Syst.*, 6, 363–380.

Barnier, B., et al. (2006), Impact of partial steps and momentum advection schemes in a global ocean circulation model at eddy-permitting resolution. *Ocean Dyn.*, 56, 543–567.

Béranger, K., L. Mortier, and M. Crépon (2005), Seasonal variability of water transport through the Straits of Gibraltar, Sicily and Corsica, derived from a high-resolution model of the Mediterranean circulation, *Prog. Oceanogr.*, 66, 341–364.

Berné, S., D. Carré, B. Loubrieu, J.-P. Mazé, L. Morvan, and A. Normand (2004), Le golfe du Lion - Carte morpho-bathymtrique, Ifremer/Conseil Régional du Languedoc-Roussillon Edition.

Bethoux, J.P. and Gentilli B., (1999), Functioning of the Mediterranean Sea: Past and Present Changes relaled to freshwater input and climatic changes. *J. Mar. Syst.* 20, 33-47.

Beuvier J (2011) Modelling the long-term variability of circulation and water masses in the Mediteranean Sea: impacts of the ocean-atmosphere exchanges: PhD Thesis. Ecole Polytechnique, Palaiseau, France. 290 p.

Beuvier, J. (2008). Modelling the long-term variability of circulation and water masses in the Mediterranean Sea: impacts of the ocean-atmosphere exchanges. PhD thesis, Physics specialty, Mechanics department, Ecole Polytechnique, Palaiseau, France, 290 pp, in French.

Beuvier, J., F. Sevault, M. Herrmann, H. Kontoyiannis, W. Ludwig, M. Rixen, E. Stanev, K. Béranger, and S. Somot (2010), Modeling the Mediterranean Sea interannual variability during 1961-2000: Focus on the Eastern Mediterranean Transient. *J. Geophys. Res.*, 115 (C08017), doi:10.1029/2009JC005950.

Beuvier J., Béranger K., Lebeaupin-Brossier C., Somot S., Sevault F., Drillet Y., Bourdallé-Badie R., Ferry N. and Lyard F. (2012) Spreading of the Western Mediterranean Deep Water after winter 2005: time scales and deep cyclone transport. *J. Geophys. Res.-Oceans.* doi:10.1029/2011JC007679.

Blanke, B., and P. Delecluse (1993), Low frequency variability of the tropical Atlantic Ocean simulated by a general circulation model with mixed layer physics, *J. Phys. Oceanogr.*, 23, 1363–1388.

Bormans, M., C. Garrett, and K. R. Thompson (1986). Seasonal variability of the surface inflow through the Strait of Gibraltar, *Oceanol. Acta*, 9, 403–414.

Bozec, A., P. Bouruet-Aubertot, D. Iudicone, and M. Crépon (2008), Impact of penetrative solar radiation on the diagnosis of water mass transformation in the Mediterranean Sea, *J. Geophys. Res.*, 113, C06012, doi:10.1029/2007JC004606.

Bryden, H. L. and Stommel, H. M., (1984). Limiting processes that determine basic features of the circulation in the Mediterranean Sea. *Oceanol. Acta*, 7, 3, 289-296.

Bryden, H. L., J. Candela, and T. H. Kinder, (1994). Exchange through the Strait of Gibraltar, *Prog. Oceanogr.* 33, 201–248.

Cazenave, A., Bonnefond, P., Mercier, F., Dominh, K. and Toumazou, V., (2002). Sea level variations in the Mediterranean Sea and Black Sea from satellite altimetry and tide gauges. *Glob. Planet. Change* 34, 59–86.

CLIPPER Project Team (1999), Modélisation à haute résolution de la circulation dans l'océan Atlantique forcée et couplée océan-atmosphère, *Sci. Tech. Rep.* CLIPPER-R3-99, Ifremer, Brest, France.

Criado-Aldeanueva F., Del Río Vera J. and García-Lafuente J., (2008). Steric and mass induced Mediterranean sea level trends from 14 years of altimetry data. *Glob. Planet. Change* 60, 563-575.

Criado-Aldeanueva, F., Soto-Navarro, J. and García-Lafuente, J., (2012). Seasonal and interannual variability of surface heat and freshwater fluxes in the Mediterranean Sea: budgets and Exchange through the Strait of Gibraltar. *Int. J. Climatol*. 32, 286-302.

Daget, N., A. T. Weaver, and M. A. Balmaseda (2009), Ensemble estimation of background-error variances in a three-dimensional variational data assimilation system for the global ocean. *Q. J. R. Meteorol. Soc.*, 135, 1071–1094.

Decharme, B., R. Alkama, H. Douville, M. Becker and A. Cazenave (2010). Global Evaluation of the ISBA-TRIP Continental Hydrological System. Part II: Uncertainties in River Routing Simulation Related to Flow Velocity and Groundwater Storage. *J. Hydrometeor*, **11**, 601–617. doi: http://dx.doi.org/10.1175/2010JHM1212.1.

Déqué, M., and J. Piedelievre (1995), High resolution climate simulation over Europe, *Clim. Dyn.* 11, 321–339.

Dussin R. and Treguier A. M., (2010) Evaluation of the NATL12-BRD81 simulation, LPO internal Report 10-03.

Drillet, Y., R. Bourdallé-Badie, L. Siefridt, and C. Le Provost (2005), Meddies in the Mercator North Atlantic and Mediterranean Sea eddy-resolving model, *J. Geophys. Res.* 110, C03016, doi:10.1029/2003JC002170.

Farmer D. and Armi L., (1986). The internal hydraulics of the Strait of Gibraltar and associated sills and narrows. *Oceanol. Acta.* (8), 37-46.

Ferry, N., L. Parent, G. Garric, B. Barnier, N. C. Jourdain, and the Mercator Ocean team (2010), Mercator Global Eddy Permitting Ocean Reanalysis GLORYS1V1: Description and Results, Mercator Ocean Quarterly Newsletter, #36 - January 2010, pp 15–28.

García-Lafuente, J., J. Delgado, J. M. Vargas, M. Vargas, F. Plaza, and T. Sarhan, (2002). Low-frequency variability of the exchanged flows through the Strait of Gibraltar during CANIGO, *Deep Sea Res. II*, 49, 4051– 4067.

García-Lafuente, J., Delgado, J., Sánchez-Román, A., Soto, J., Carracedo, L. and Díaz del Río, G., (2009). Interannual variability of the Mediterranean outflow observed in Espartel sill, western Strait of Gibraltar. *J. Geophys. Res.* 114 C10, doi: 10.1029/2009JC005496.

García-Lafuente, J., Sánchez-Román, A., Naranjo, C. and Sánchez-Garrido, J.C., (2011). The very first transformation of the Mediterranean outflow in the Strait of Gibraltar. *J. Geophys. Res.* 116, C07010, doi: 10.1029/2011JC006967.

Goosse, H., Selten, F.M., Haarsma, R.J. and Opsteegh, J.D., (2001). Decadal variability in high northern latitudes as simulated by an intermediate-complexity climate model *Annals of Glaciology*, 33, pp. 525-532.

Guldberg, A., E. Kaas, M. Déqué, S. Yang, and S. Vester Thorsen (2005), Reduction of systematic errors by empirical model correction: Impact on seasonal prediction skill, *Tellus, Ser. A*, 57, 575–588.

Herrmann, M., and S. Somot (2008), Relevance of ERA40 dynamical downscaling for modeling deep convection in the Mediterranean Sea, *Geophys. Res. Lett.*, 35, L04607, doi:10.1029/2007GL032442.

Herrmann M., Somot S., Sevault F., Estournel C., Déqué M. (2008) Modeling the deep convection in the Northwestern Mediterranean Sea using an eddy-permitting and an eddy-resolving model: case study of the 1986-87 winter. *J. Geophys. Res*. 113, C04011, doi:10.1029/2006JC003991

Herrmann M., Sevault F., Beuvier J., Somot S. (2010) What induced the exceptional 2005 convection event in the Northwestern Mediterranean basin ? Answers from a modeling study. *J. Geophys. Res*. , 115, doi:10.1029/2010JC006162

Herrmann M., Somot S., Calmanti S., Dubois C. and Sevault F. (2011). Representation of daily wind speed spatial and temporal variability and intense wind events over the Mediterranean Sea using dynamical downscaling : impact of the regional climate model configuration. *Nat. Hazards Earth Syst. Sci.*, 11, 1983-2001, doi:10.5194/nhess-11-1983-2011.

Kinder, T. H., and H. L. Bryden (1990), Aspiration of deep waters through straits, in The Physical Oceanography of Sea Straits, edited by L. J. Pratt, pp. 295– 319, Kluver Academic, Norwell, Mass.

Lebeaupin Brossier, C., K. Béranger, C. Deltel, and P. Drobinski (2011), The Mediterranean response to different space-time resolution atmospheric forcings using perpetual mode sensitivity simulations, *Ocean Model.*, 36, 1–25, doi:10.1016/j.ocemod.2010.10.008.

Lebeaupin Brossier, C., K. Béranger and P. Drobinski (2012). Sensitivity of the northwestern Mediterranean Sea coastal and thermohaline circulations simulated by the 1/12°-resolution ocean model NEMO-MED12 to the spatial and temporal resolution of atmospheric forcing. *Ocean Model.*, 43-44, 94-107, doi:10.1016/j.ocemod.2011.12.007.

Levitus, S., J. Antonov, and T. Boyer (2005), Warming of the world ocean, 1955-2003, *Geophys. Res. Lett.*, 32 (L02604).

López-Jurado, J.L., González-Pola, C. and Vélez-Belchí, P. (2005). Observation of an abrupt disruption of the long-term warming trend at the Balearic Sea, Western Mediterranean Sea, in summer 2005, *Geophys. Res. Lett.* 32, L24606, doi:10.1029/2005GL024430.

Ludwig, W., E. Dumont, M. Meybeck, and S. Heussner (2009), River discharges of water and nutrients to the Mediterranean and Black Sea: Major drivers for ecosystem changes during past and future decades?, *Prog. Oceanogr.* 80, 199–217.

Lyard, F., F. Lefevre, T. Letellier, and O. Francis (2006), Modelling the global ocean tides: modern insights from FES2004, *Ocean Dyn.* 56 (5-6), doi:10.1007/s10236- 006-0086-x.

Madec, G. (2008), NEMO ocean engine, Note Pôle Model. 27, Inst. Pierre-Simon Laplace des Sci. de l'Environ., Paris, France.

Mariotti, A., Struglia, M.V., Zeng, N. and Lau, K.-M., (2002). The hydrological cycle in the Mediterranean region and implications for the water budget of the Mediterranean Sea. *J. Climate* 15, 1674–1690.

Mariotti A., (2011). Recent Changes in the Mediterranean Water Cycle: A Pathway toward Long-Term Regional Hydroclimatic Change, *J. Clim*. 23, 1513-1525. doi:10.1175/2009JCLI3251.1.

MEDAR-MEDATLAS Group (2002), MEDAR/MEDATLAS 2002 database, Cruise inventory, observed and analysed data of temperature and bio-chemical parameters [CD-ROM], Ifremer, Brest, France.

Medimap Group (2005), Morpho-bathymetry of the Mediterranean Sea, CIESM/Ifremer Edition, 2 maps at 1/2000000.

Millot, C., Candela, J., Fuda, J. L. and Tber, Y. (2006), Large warming and salinification of the Mediterranean outflow due to changes in its composition, *Deep Sea Res. I*, 53, 656–666.

Naranjo, C., García-Lafuente, J., Sánchez-Garrido, J,C., Sánchez-Román, A. and Delgado-Cabello, J. (2012).The western alboran gyre helps ventilate the western mediterranean deep water through Gibraltar. *Deep Sea Res. I* 63, 157-163.

Oguz, T., and Sur, H. I., (1989), A two-layer model of water exchange through the Dardanelles Strait, *Oceanol. Acta*, 12, 23–31.

Oki, T. and Sud, Y. C. (1998), Design of Total Runoff Integrating Pathways (TRIP) - A global river channel network. *Earth Interact.* 2.

Oddo P., M. Adani N. Pinardi, C. Fratianni, M. Tonani, D. Pettenuzzo (2009). A Nested Atlantic-Mediterranean Sea General Circulation Model for Operational Forecasting. *Ocean Sci. Discuss.*, 6, 1093-1127

Parrilla, G., T. H. Kinder, and R. H. Preller (1986), Deep and intermediate Mediterranean water in the western Alboran Sea. *Deep Sea Res. I*, 33, 55– 88.

Reynaud, T., P. Legrand, H. Mercier, and B. Barnier (1998), A new analysis of hydrographic data in the Atlantic and its application to an inverse modeling study, Int. WOCE Newsl., 32, 29–31.

Rixen, M., Bechers, J.M., Levitus, S., Antonov, J., Boyer, T., Maillard, C., Fichaut, M., Balopoulos, M., Iona, S., Dooly, S., García, M.J., Manca, B., Giorgetti, A., Manzella, G., Mikhailov, N., Pinardi, N. and Zavatereli, M. (2005), The western Mediterranean deep water: A proxy for climate change. *Geophys. Res. Lett.* 32, LI2608.

Roullet, G., and G. Madec (2000), Salt conservation, free surface, and varying levels: A new formulation for ocean general circulation models, *J. Geophys. Res.* 105, 23,927–23,942.

Sánchez-Garrido, J. C., Sannino, G., Liberti, L., García-Lafuente, J. and Pratt, L. (2011). Numerical modeling of three-dimensional stratified tidal flow over Camarinal Sill, Strait of Gibraltar. *J. Geophys. Res.*, 116, 1-17.

Sanchez-Román A., Sannino G., García-Lafuente J., Carillo A. and Criado-Aldeanueva F., (2009). Transport estimates at the western section of the Strait of Gibraltar: A combined experimental and numerical modeling study. *J. Geophys. Res.* (114), C06002, doi:10.1029/2008JC005023.

Sannino G., Herrmann M., Carillo A., Rupolo V., Ruggiero V., Artale V. and Heimbach P., (2009). An eddy-permitting model of the Mediterranean Sea with a two-way grid refinement at the Strait of Gibraltar. *Ocean Model.* (30), 56-72.

Schroeder K., A. Ribotti, M. Borghini, R. Sorgente, A. Perilli and G.P. Gasparini, (2009). An extensive western Mediterranean deep water renewal between 2004 and 2006. *Geophys. Res. Lett.* 35(18), L18605.

Sevault, F., S. Somot, and J. Beuvier (2009), A regional version of the NEMO ocean engine on the Mediterranean Sea: NEMOMED8 user's guide, Note Cent. 107, Groupe de Meteorol. de Grande Echelle et Clim., Cent. Natl. de Rech. Meteorol., Toulouse, France.

Simmons, A., and J. Gibson (2000), The ERA40 project plan, ERA40 Proj. Rep. 1, Eur. Cent. for Medium-Range Weather Forecasts, Reading, U. K.

Smith, W. H. F., and D. T. Sandwell (1997), Global sea floor topography from satellite altimetry and ship depth sounding, *Science* 277, 1956–1962.

Somot, S., F. Sevault, and M. Déqué (2006), Transient climate change scenario simulation of the Mediterranean Sea for the twenty-first century using a high-resolution ocean circulation model, *Clim. Dyn.* 27, 851–879.

Soto-Navarro, J., F. Criado-Aldeanueva, J. García-Lafuente, and A. Sánchez-Román (2010), Estimation of the Atlantic inflow through the Strait of Gibraltar from climatological and in situ data, *J. Geophys. Res.* 115 (C10023), doi:10.1029/2010JC006302.

Stanev, E. and Peneva, E. L. (2002). Regional sea level response to global climatic change: Black Sea examples. *Glob. Planet. Change.* 32, 33-47.

Stanev, E. V., P.-Y. Le Traon, and E. L. Peneva (2000), Sea level variations and their dependency on meteolorogical and hydrological forcing: Analysis of altimeter and surface data for the Black Sea, *J. Geophys. Res.* 105, 17,203–17,216.

Stommel, H., H. Bryden, and P. Mangelsdorf (1973), Does some of the Mediterranean outflow come from great depth? *Pure Appl. Geophys.*, 105, 879–889.

Thorpe R.B. and Bigg G.R. (2000) Modelling the sensitivity of the Mediterranean outflow to anthropogenically forced climate change. *Clim. Dyn.*, 16 (2000), pp. 355–368

Tonani, M., N. Pinardi, S. Dobricic, I. Pujol, and C. Fratianni (2008), A high-resolution free-surface model of the Mediterranean Sea. *Ocean Science*, 4, 1–14.

Tsimplis, M., M. Marcos, J. Colin, S. Somot, A. Pascual, and A. G. P. Shaw (2009), Sea level variability in the Mediterranean Sea during the 1990s on the basis of one 2D and one 3D model, *J. Mar. Syst.* 78, 109–123.

Valcke, S. (2006). OASIS3 User Guide (prism_2-5). CERFACS Technical Report TR/CMGC/06/73, PRISM Report No 3, Toulouse, France. 60 pp.

Vlassenko, V., Sánchez-Garrido, J. C., Stashchuk, N., García-Lafuente, J. and Losada, M. (2009). Three-dimensional evolution of large amplitude internal waves in the Strait of Gibraltar. *J. Phys. Oceanogr.*, 39, 2230-2246.

Vörösmarty, C., B. Fekete, and B. Tucker (1996), Global River Discharge Database, RivDis, http://www.rivdis.sr.unh.edu/, U. N. Educ. Sci. and Cult. Organ. Paris.

TABLES

	ΔT (s)	grid	bathymetry	T, S initial state	Atmospheric forcing	Period
NM8-NOSSH	1200	1/8ºx1/8º + stretched at Gibraltar	ETOPO5	MEDATLAS + anomalies 1960-1962	ARPERA-V2	1961-2008
NM8	1200	1/8ºx1/8º+ stretched at Gibraltar	ETOPO5	NM8-NOSSH	ARPERA-V2	2002-2008
NM12-ARP	720	ORCA-1/12º (6-8km)	Mercator-LEGOS	MEDATLAS + anomalies 1997-1999	ARPERA-V2	2002-2008
NM12-ARP-2DE	720	ORCA-1/12º (6-8km)	Mercator-LEGOS	MEDATLAS + anomalies 1997-1999	ARPERA-V2	2002-2008
NM12	720	ORCA-1/12º (6-8km)	Mercator-LEGOS	MEDATLAS + anomalies 1997-1999	ARPERA-V2	2002-2008
NM12-ECMWF	720	ORCA-1/12º (6-8km)	Mercator-LEGOS	MEDATLAS + anomalies 1997-1999	ECMWF	2002-2007
NM36	240	ORCA-1/36º (2-3km)	Mercator-LEGOS	NM12-ECMWF	ECMWF	2003-2007

Table 1. Characteristics of the different simulations used in the study. The bathymetries of ETOPO5 or Mercator-LEGOS have been interpolated onto the NM8, NM12 or NM36 grids. The initial states come from the MEDATLAS climatology for which anomalies (Rixen et al. 2005) have been added in a 3-year window around the starting date.

	C_D ($\cdot 10^{-3}$)	E	SSH in the Atlantic buffer zone	T,S in the Atlantic buffer zone	TD	MD ($\cdot 10^{-10}$)	VD
NM8-NOSSH	1.225	$2.5\ 10^{-3}$	NO	Reynaud + anomalies of Daget	125	-1	50
NM8	1.225	$2.5\ 10^{-3}$	GLORYS1V1	Reynaud + anomalies of Daget	125	-1	50
NM12-ARP	1	$2.5\ 10^{-3}$	NO	Levitus	60	-1.25	10
NM12-ARP-2DE	1	2D field	GLORYS1V1	Levitus	60	-1.25	10
NM12	1	2D field	GLORYS1V1	Levitus	60	-1.25	10
NM12-ECMWF	1	2D field	GLORYS1V1	Levitus	60	-1.25	10
NM36	1	2D field	GLORYS1V1	Levitus	30	-10	10

Table 2. Parameterizations for the different simulations used in the study. Concerning the bottom friction, C_D is the drag coefficient and E the bottom turbulent kinetic energy background (constant or a 2D field; m^2/s^2). To assure the model volume conservation, the SSH of the model in the Atlantic buffer zone is relaxed towards a climatological SSH from the GLORYSV1 reanalysis, except for NM8-NOSSH and NM12-ARP, for which the net evaporation over the Mediterranean area is added as precipitation at each time step. The tracer diffusion is made through a laplacian operator along iso-neutral surfaces with a coefficient TD (m^2/s). The momentum diffusion is applied with a biharmonic operator with a coefficient MD (m^2/s). The turbulent closure scheme TKE of NEMO is used and the vertical diffusion is enhanced towards a maximum value VD in case of instability.

	Longitude	Latitude	Depth (m)
ES	5º 58.6’ W	35º 57.1’ N	356
NEMOMED8	5º 56.22’ W	35º 51.1’ N	292
NEMOMED12	5º 56.04’ W	35º 54’ N	266
NEMOMED36	5º 59.58’ W	35º, 50’ N	318

Table 3. Positions and depth of ES and the model grid points used in the evaluation.

	NM8-NOSSH	NM8	NM12	NM12-ARP	NM12-ARP-2DE	NM12-ECMWF	NM36
Monthly outflow time series	0.40	0.34	0.28	0.22	0.19	0.30	0.32
12-Month seasonal cycle outflow	0.71	0.75	0.57	0.34	0.48	0.30	0.64
12-Month seasonal cycle inflow	0.57	0.88	0.80	0.68	0.72	0.62	0.80

Table 4. Correlation between the observations and simulations, computed in the common period for each simulation. First row shows the outflow monthly time series. Second and third rows show the month to month correlation of the outflow and inflow seasonal cycle.

	Obs.	**NM8-NOSSH**	**NM8**	**NM12**	**NM12-ARP**	**NM12-ARP-2DE**	**NM12-ECMWF**	**NM36**
Outflow (Sv)	**-078±0.06**	-0.79±0.07	-0.78±0.07	-0.69±0.07	-0.69±0.07	-0.68±0.08	-0.69±0.06	-0.63±0.04
Inflow (Sv)	0.81±0.05*	0.85±0.09	0.8±0.2	0.73±0.09	0.73±0.06	0.73±0.09	0.74±0.07	0.68±0.07
Net flow (Sv)	0.04±0.04*	0.05±0.02	0.06±0.09	0.05±0.06	0.05±0.02	0.05±0.02	0.05±0.06	0.05±0.06
E-P-R-B	0.05±0.02*	0.05±0.03	0.05±0.03	0.04±0.03	0.05±0.04	0.05±0.04	0.05±0.03	0.05±0.03

Table 5. Mean inflow, outflow and net flow at the Strait of Gibraltar for the observations and the different simulations, computed in their common periods. The values of the observed inflow and net flow, marked with an asterisk (*), are those indirectly obtained by Soto-Navarro et al. (2010). The error intervals are the standard deviation of the monthly time series. E-P-R-B is the mean water deficit for the whole basin.

		Salinity	Temperature (ºC)
Observations	LIW	38.56	13.22
	WMDW	38.45	12.8
	NACW	36.2	15.0
NM8	LIW	[38.63, 38.68]	[13.68,13.88]
	WMDW	[38.43, 38.45]	[12.76, 12.80]
	NACW	[36.18, 36.12]	[14.44, 14.88]
NM12	LIW	[38.50, 38.52]	[13.12, 13.18]
	WMDW	38.44	[12.76, 12.77]
	NACW	36.33	[15.20, 15.25]
NM36	LIW	[38.51, 38.54]	[13.11, 13.24]
	WMDW	38.44	[12.76, 12.77]
	NACW	[36.15, 36.26]	[15.13, 15.21]

Table 6. Thermohaline characteristics of the LIW, WMDW and NACW water masses used as reference for the estimation of their respective fraction in the composition of the outflow. For the observation historical literature values are used while for the models different values are obtained for each year (see text). The intervals correspond to the minimum and maximum values for the simulated period.

FIGURES

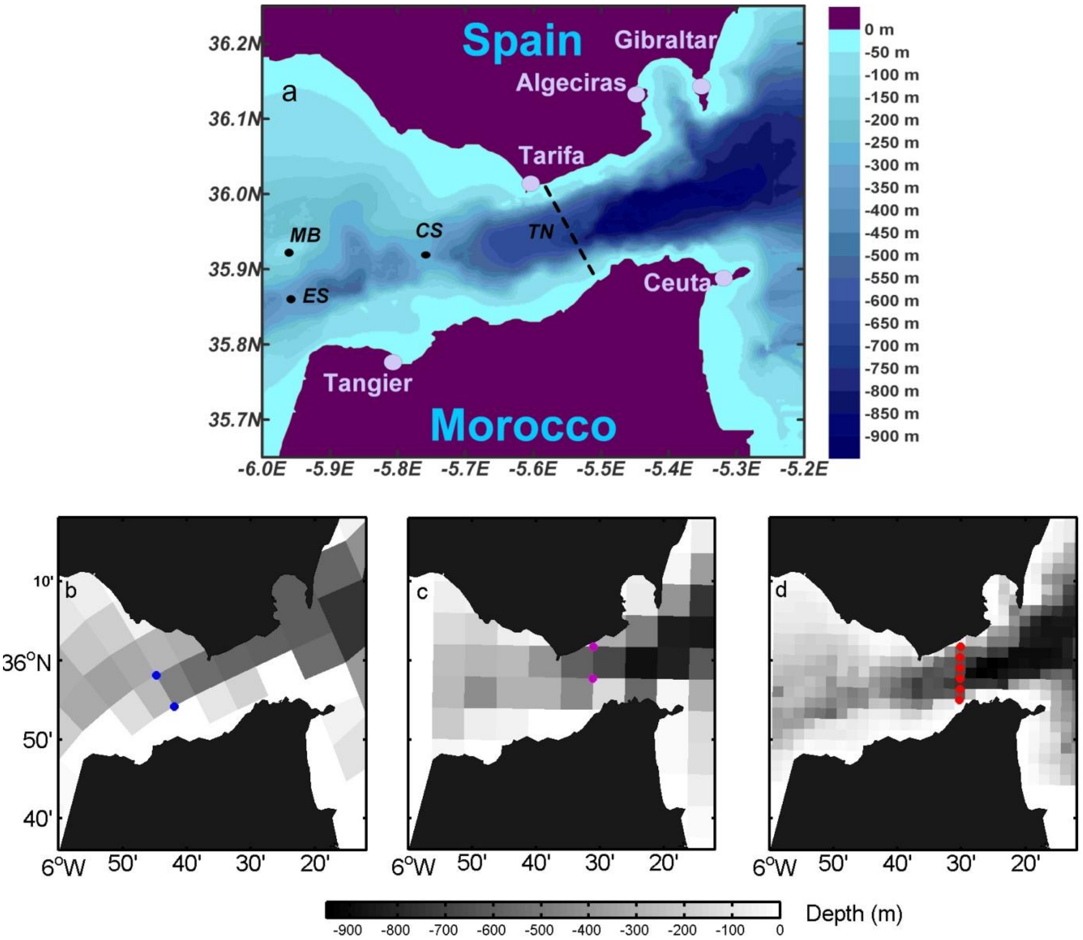

Figure 1. a) Bathymetric map of the Strait of Gibraltar showing the main topographic features. CS and ES indicate the location of the sills of Camarinal and Espartel, respectively. MB is the submarine ridge of Majuan bank and TN the Tarifa Narrows. **b) – d).** Bathymetry at the Strait of Gibraltar for NEMOMED8 (b), NEMOMED12 (c) and NEMOMED36 (d). The color points represent the grid points where the transport is estimated on each model.

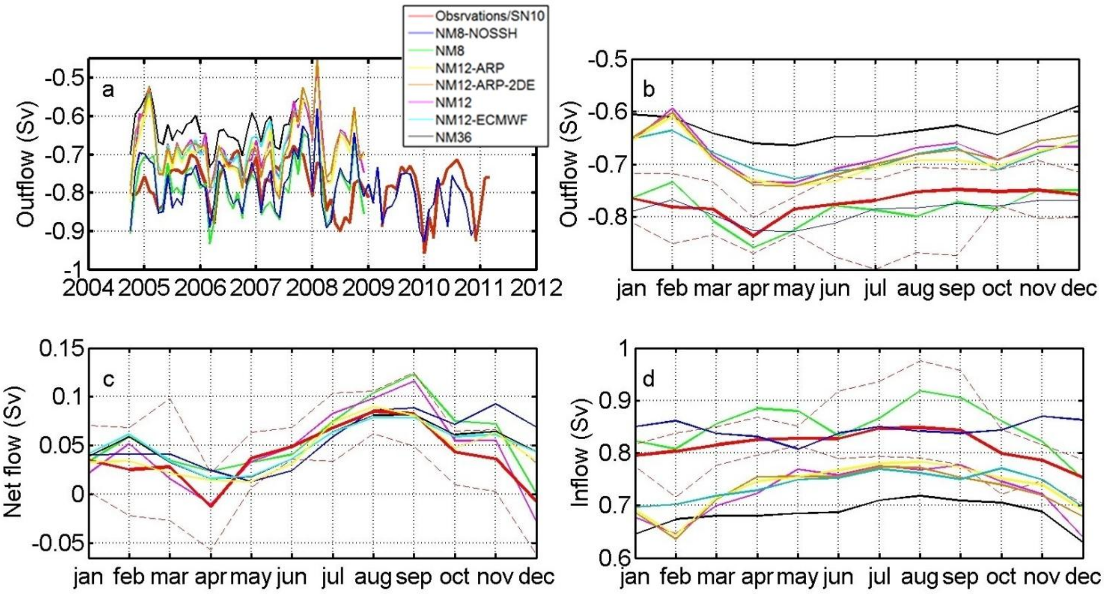

Figure 2. a) Monthly mean time series of the outflow for the observations and the different simulations. **b)** Monthly mean seasonal cycle of the outflow for the observations and the different simulations computed in their comon periods.. **c)** Monthly mean seasonal cycle of the net flow for the observations and the different simulations. **d)** Monthly mean seasonal cycle of the inflow for the observations and the different simulations. In all figures solid lines represent: Observations (red), NM8-NOSSH (blue), NM8 (green), NM12-ARP (yellow), NM12-ARP-2DE, NM12 (magenta), NM12-EMWF (light blue) and NM36 (black). The dashed lines correspond to the maximum and minimum values of every month for the observations. The observed inflow and net flow are those indirectly estimated by Soto-Navarro et al., (2010).

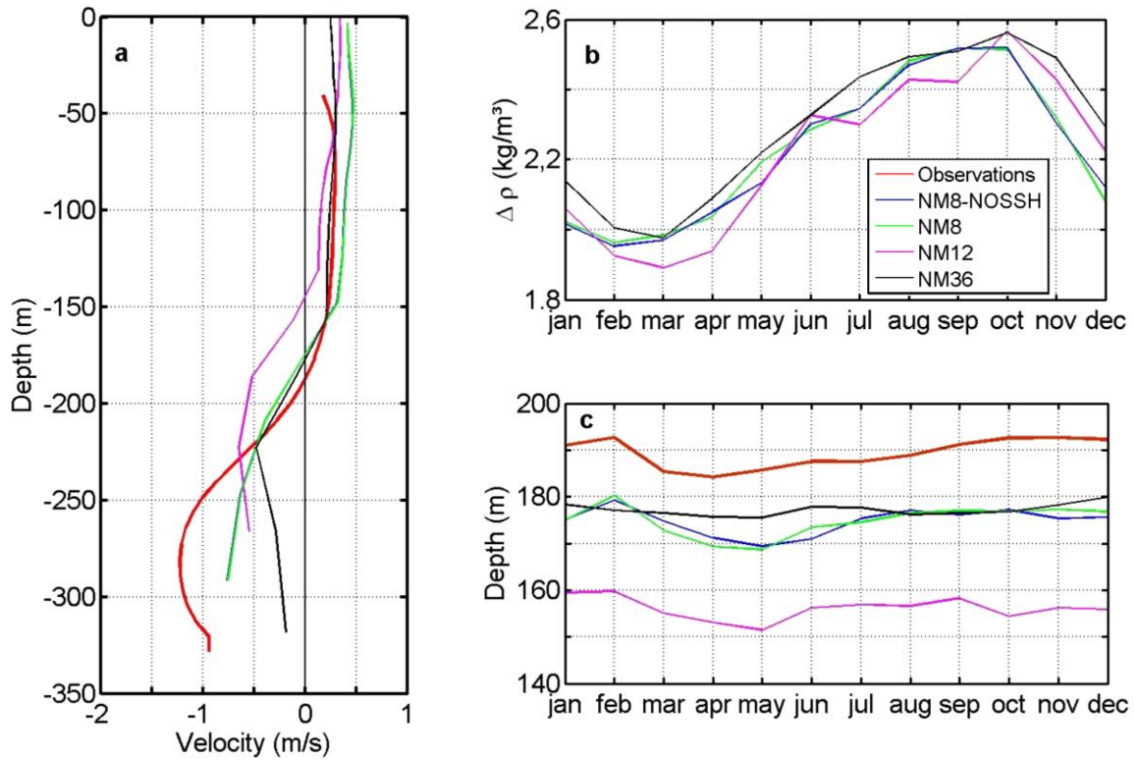

Figure 3. a) Mean velocity profile at ES for the observations and the different simulations. **b)** Mean seasonal cycle of the density difference between the Mediterranean and Atlantic layers. **c)** Mean seasonal cycle of the interface depth at ES for the observations and the different simulations. In all figures solid lines represent: Observations (red), NM8-NOSSH (blue), NM8 (green), NM12 (magenta) and NM36 (black).

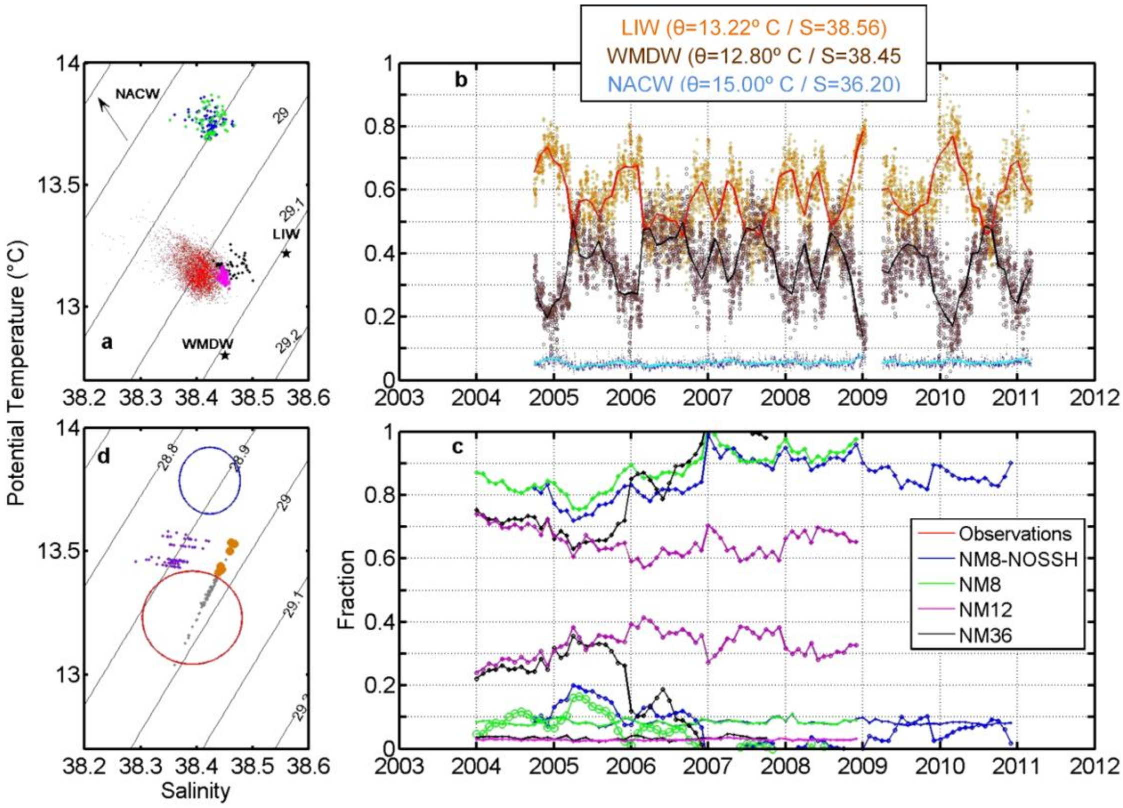

Figure 4. a) θ-S diagram of the outflowing waters for the observations and the different simulations at ES. Colors correspond to: Observations (red), NM8-NOSSH(blue), NM8 (green), NM12 (magenta) and NM36 (black). Black stars are the reference points for the LIW and WMDW used in the decomposition and specified in table 5. The NACW point is out of the diagram. **b)** Fraction of LIW (orange diamonds), WMDW (brown circles) and NACW (blue points), present in the Mediterranean outflow measured at ES. Thick lines are the monthly means. **c)** Fraction of LIW (diamonds), WMDW (circles) and NACW (points) in the Mediterranean outflow for the different simulations. The colors represent the same as in a). **d)** Results of the water mass fraction tests for NM8. Grey points are the θ-S values when the fraction of NACW is forced to be 0.05, purple points are the values when the WMDW fraction is forced to be 0.35 and orange points result when both conditions are imposed at the same time. The red circle indicates the position of the ES data and the blue one the original position of the NM8 points.

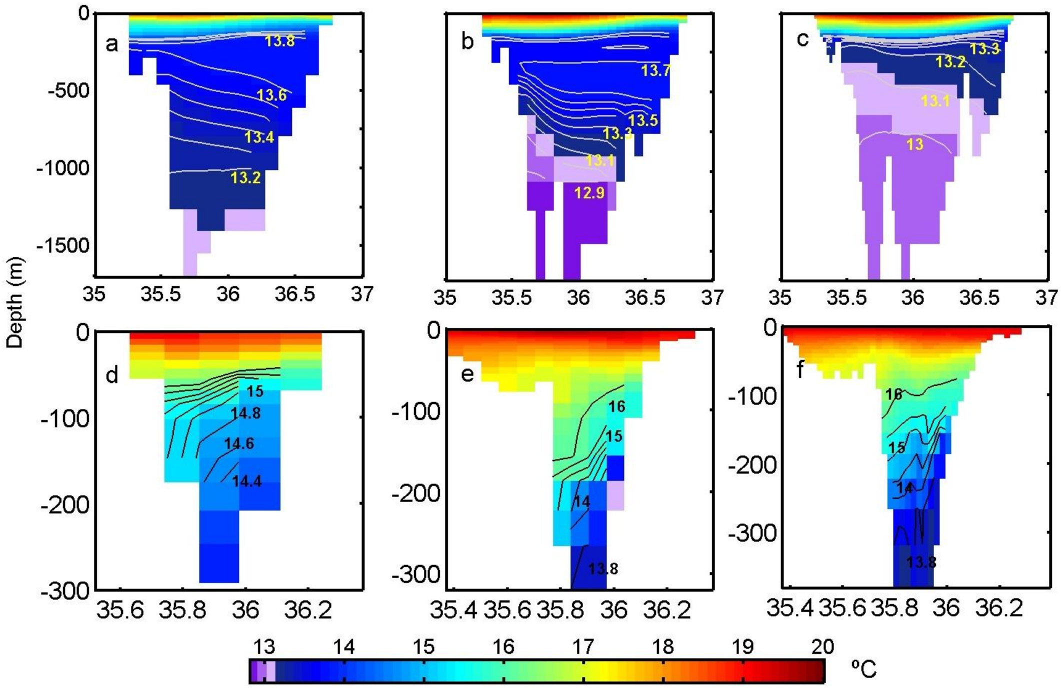

Figure 5. Temperature cross section at the Alboran Sea (4ºW) and at the western boundary of the Strait of Gibraltar (6ºW) for NM8 (a, d), NM12 (b, f) and NM36 (c, f). Lines indicate isotherms.

Figure 1

Click here to download high resolution image

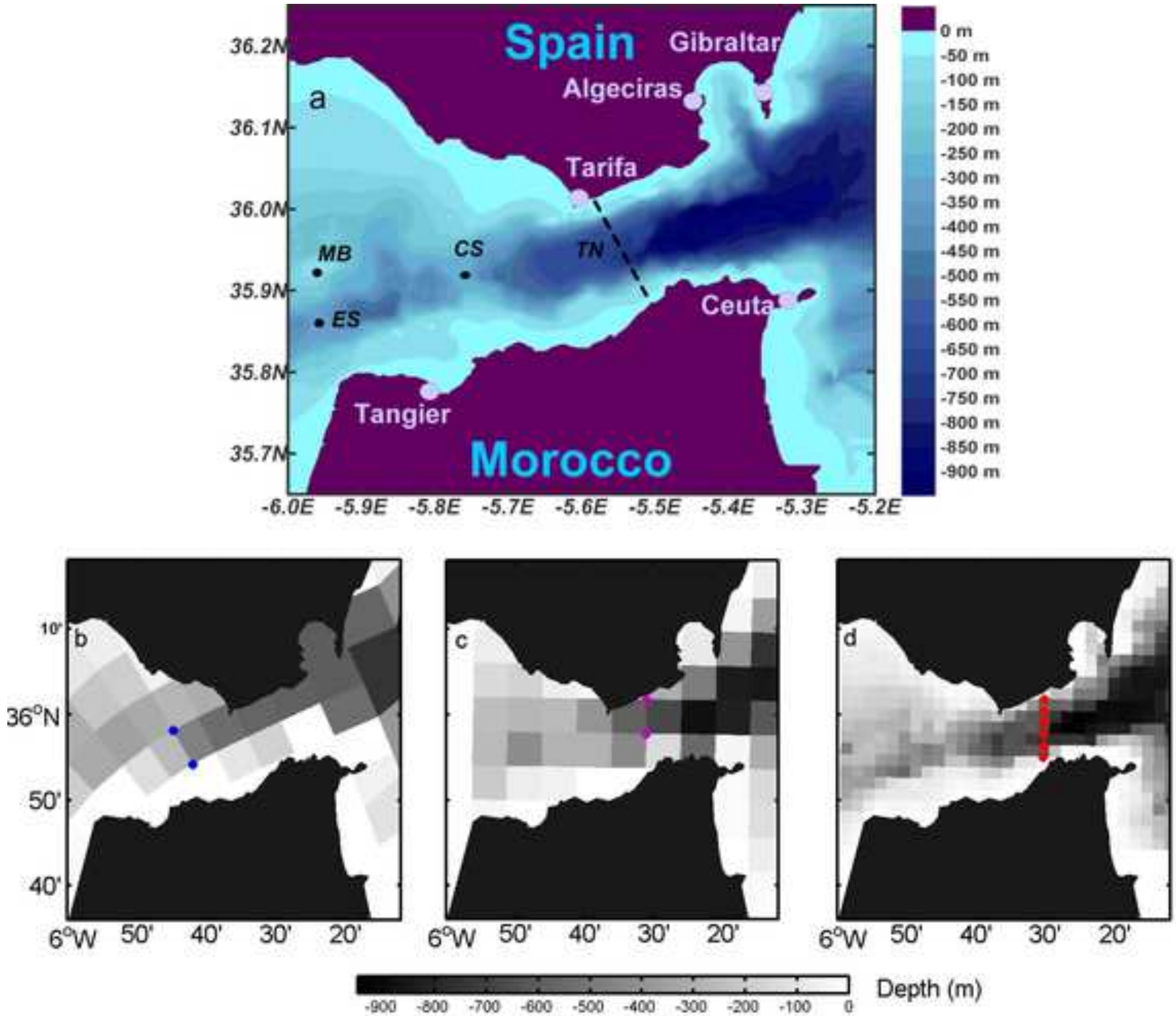

Figure 2
Click here to download high resolution image

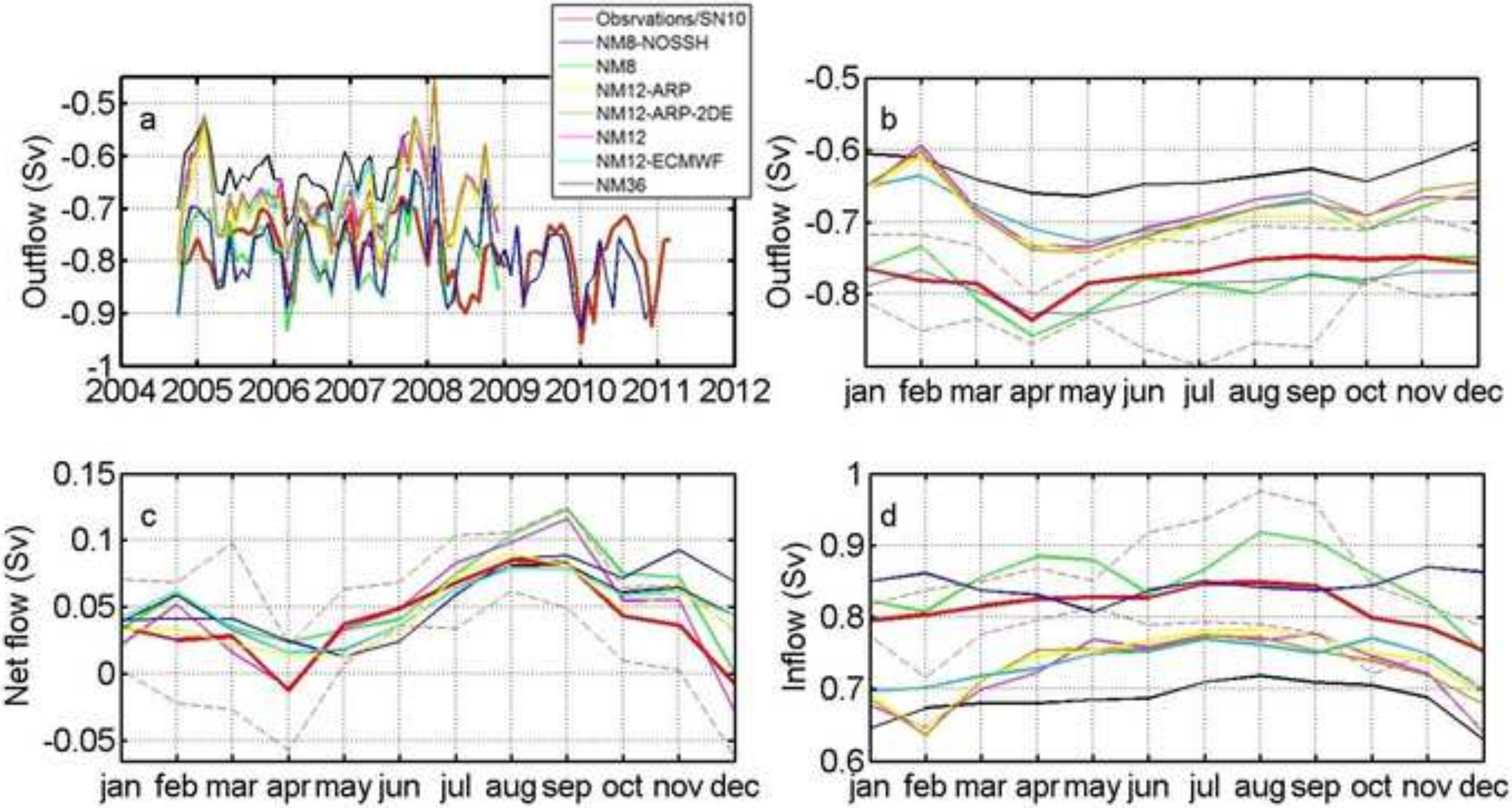

Figure 3
Click here to download high resolution image

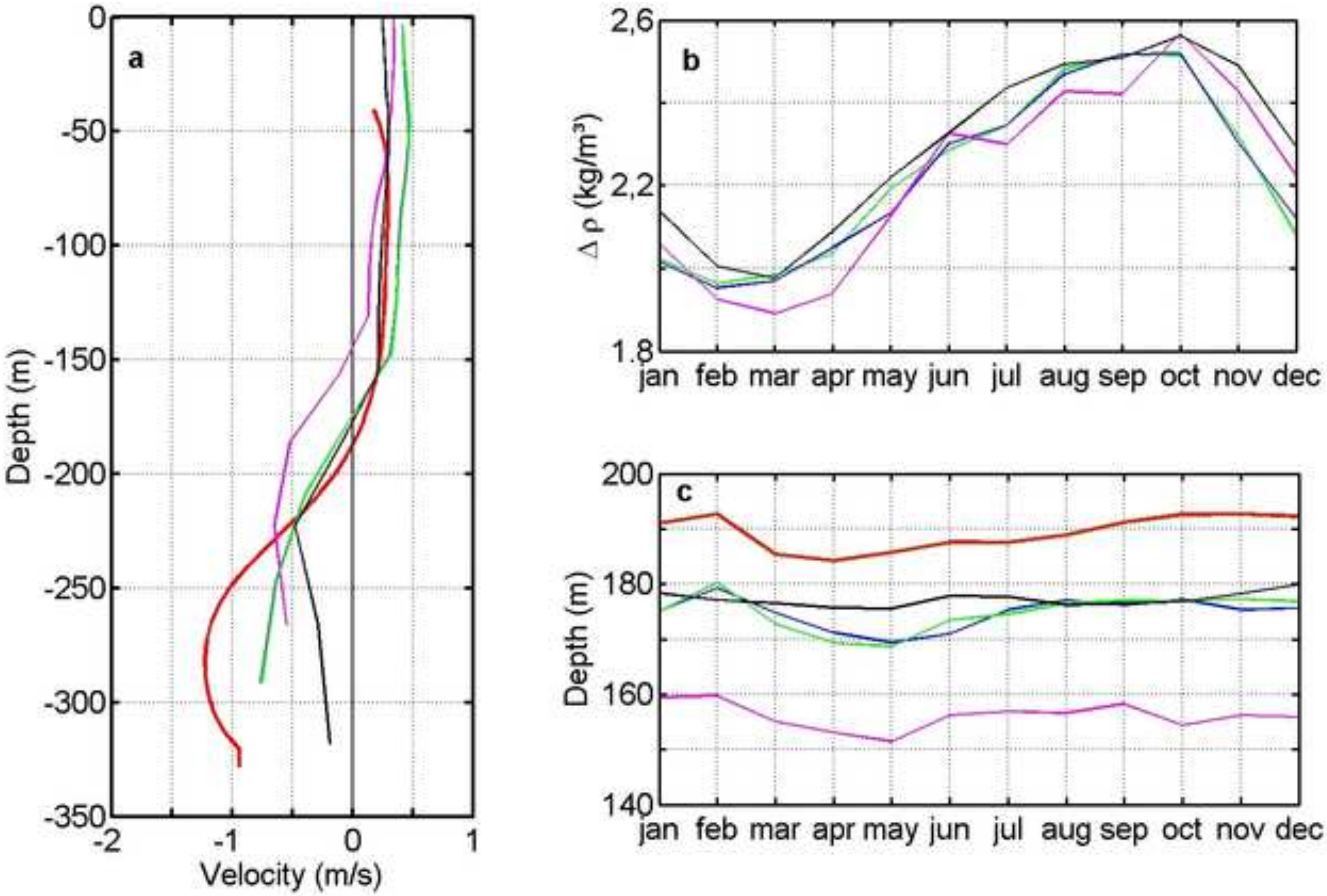

Figure 4
Click here to download high resolution image

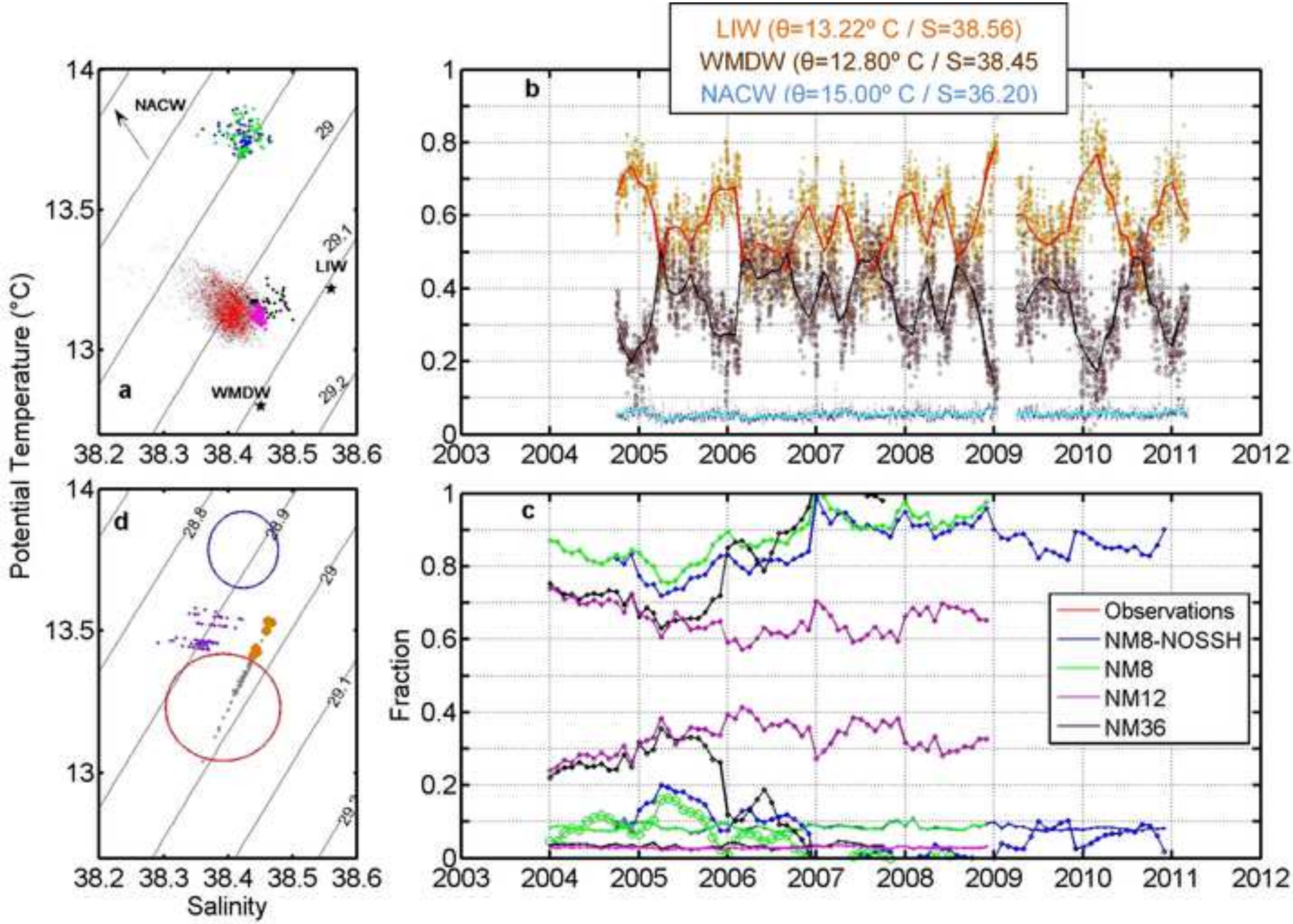

Figure 5
Click here to download high resolution image